Chinese Journal of Chemical Engineering 65 (2024) 29–34

Contents lists available at ScienceDirect

Chinese Journal of Chemical Engineering

journal homepage: www.elsevier.com/locate/CJChE

Full Length Article

Solubility of iron(III) and nickel(II) acetylacetonates in supercritical carbon dioxide

Haixin Sun [1], Jianlei Qi [2], Jianfei Sun [1], Lin Li [1], Kunpeng Yu [1], Jintao Wu [1], Jianzhong Yin [1,*]

[1] State Key Laboratory of Fine Chemicals, School of Chemical Engineering, Dalian University of Technology, Dalian 116024, China
[2] College of Chemical Engineering, Inner Mongolia University of Technology, Hohhot 010051, China

ARTICLE INFO

Article history:
Received 21 April 2023
Received in revised form 9 July 2023
Accepted 12 July 2023
Available online 17 July 2023

Keywords:
Iron(III) acetylacetonate
Nickel(II) acetylacetonate
Supercritical carbon dioxide
Solubility measurement
Correlation model
Phase equilibrium

ABSTRACT

As a common precursor for supercritical CO_2 ($scCO_2$) deposition techniques, solubility data of organometallic complexes in $scCO_2$ is crucial for the preparation of nanocomposites. Recently, metal acetylacetonates have shown great potential for the preparation of single-atom catalytic materials. In this study, the solubilities of iron(III) acetylacetonate ($Fe(acac)_3$) and nickel(II) acetylacetonate ($Ni(acac)_2$) were measured at the temperature from 313.15 to 333.15 K and in the pressure range of 9.5–25.2 MPa to accumulate new solubility data. Solubility was measured using a static weight loss method. The semi-empirical models proposed by Chrastil and Sung *et al.* were used to correlate the solubility data of $Fe(acac)_3$ and $Ni(acac)_2$. The equations obtained can be used to predict the solubility of the same system in the experimental range.

1. Introduction

Carbon dioxide is the most widely used supercritical fluid (SCF) because of its non-toxicity, non-flammability, low cost, and moderate critical pressure and temperature [1]. The solubility of metal complexes in supercritical carbon dioxide ($scCO_2$) was initially investigated for applications in the development of supercritical fluid extraction processes for metals [2–5]. It was then extended to applications such as materials processing and chemical reactions [6–10]. Recently, metal acetylacetonate has been used as the precursor for $scCO_2$ deposition processes to prepare single-atom catalytic materials [11,12].

The solubility of organometallic complexes in $scCO_2$ is very important in practical applications and has been reported in some literature [13–16]. Ashraf-Khorassani *et al.* [17] described the dynamic and static solubility experimental techniques for measuring the solubility of compounds in SCF. In addition, four other conventional analytical techniques are frequently used to determine solubility in SCF, including: gravimetric [18], chromatographic [19,20], spectroscopic [21,22], and piezoelectric methods [23]. Škerget *et al.* [24] and Rad *et al.* [25] summarized the semi-empirical models most popular used to correlate the solubility of solids in SCF, and solubility data for organometallic compounds can also be found directly in the literature [24,26,27].

The solubility behavior of metal complexes in $scCO_2$ is affected by the metals involved and their ligand side-chains [26]. Aschenbrenner *et al.* [28] determined the solubility of various metal cyclopentadienyl (cp) complexes in $scCO_2$ with a dynamic-gravimetric method at 333 K. The metal complexes were in increasing order of solubility as $Cr(cp)_2 < Ni(cp)_2 < Co(cp)_2 < Fe(cp)_2$. Among the various types of organic ligands used in many research and industrial fields, β-diketonate is the most extensively studied ligand in $scCO_2$. The most several recently studied β-diketonates include acetylacetonate (acac), 2,2,6,6-tetramethyl-3,5-heptanedioate (thd), and hexafluoroacetylacetonate (hfac) [27]. Most of the investigated acac complexes generally exhibit only low solubility in $scCO_2$ compared with thd and hfac complexes. Haruki *et al.* [29] utilized a circulation-type apparatus with *in situ* UV–Vis spectrometry to determine the solubility of $Cu(acac)_2$, $Co(acac)_2$, $Cu(thd)_2$, and $Co(thd)_2$ in $scCO_2$. The metal complexes were ordered in increasing solubility as $Cu(acac)_2 < Co(acac)_2 < Cu(thd)_2 < Co(thd)_2$. Lagalante *et al.* [30] reported the solubility of 10 copper(II) β-diketonate complexes in $scCO_2$ at 313 K. The solubilities of $Cu(acac)_2$, $Cu(thd)_2$ and $Cu(hfa)_2$ were ranked second, sixth and tenth in increasing order, respectively.

Data on the solubility of metal acetylacetonates in $scCO_2$ is relatively scarce, especially considering their solubility in $scCO_2$. The solubilities of $Fe(acac)_3$ in $scCO_2$ at 313 K and 333 K were

* Corresponding author.
E-mail address: jzyin@dlut.edu.cn (J. Yin).

https://doi.org/10.1016/j.cjche.2023.07.001
1004-9541/

determined by Roggeman *et al.* [31] and Haruki *et al.* [32] using spectroscopic and semi-intermittent flow methods, respectively. Andersen *et al.* [33] measured the solubilities of $Fe(acac)_3$ by near-infrared spectroscopy from 313 to 333 K with a high-pressure photocell. Data on the solubility of $Ni(acac)_2$ in $scCO_2$ is more limited. Kersch *et al.* [34] measured the solubility of mixtures of $Ni(acac)_2$ with other metal acetylacetonates, such as $Cu(acac)_2$, at 313 K, 16 MPa. The usage of the mixture resulted in the experimental solubility of $Cu(acac)_2$ about one order of magnitude lower than that reported in the literature. Aschenbrenner *et al.* [28] determined the solubility of $Ni(acac)_2$ with a dynamic-gravimetric method at 333 K.

The application of metal complexes in $scCO_2$ is gradually expanding. In this study, the solubilities of $Fe(acac)_3$ and $Ni(acac)_2$ in $scCO_2$ were measured several times at 313.15, 323.15 and 333.15 K with a static weight loss method to provide basic data for subsequent applications [35]. Finally, the experimental data was correlated using the semi-empirical model proposed by Chrastil [36] and Sung and Shim [37] respectively.

2. Materials and Methods

2.1. Materials

$Fe(acac)_3$ (analytically pure, >98%) and $Ni(acac)_2$ (analytically pure, >95%) were purchased from Shanghai Aladdin Biochemical Technology Co., Ltd. Pure CO_2 (>99.99%) was purchased from Dalian Junfeng Gas Co., Ltd. Deionized water was obtained by reverse osmosis and subsequent ion exchange. Ethanol (EtOH, analytically pure, >99.5%) was purchased from Tianjin Fuyu Fine Chemical Co., Ltd. Deionized water and ethanol were only used for washing. All materials were used without further purification. Further, the chemical structures of the metal complexes are illustrated in Fig. 1.

2.2. Apparatus and procedure

The experimental equipment (Fig. 2) consists of four main parts: CO_2 cylinder, CO_2 pressurization system comprising a cooling coil and a high pressure liquid chromatography (HPLC) pump, a system for measuring the solubility, and cold trap for residue collection. The system temperature was controlled by a thermostatic blast drying oven with an uncertainty of ±0.1 K. The system pressure was regulated using the HPLC pump with an accuracy of approximately ± 0.01 MPa, and measured by the pressure sensor connected to the digital indicator. During each measurement, the sample was weighed on a balance with a minimum scale of 10^{-4} g and an accuracy of 10^{-3} g. The volume of the stainless steel vessel was 7.3×10^{-2} L. Therefore, the lower limit of solubility measurement was 1.37×10^{-2} g·L^{-1}.

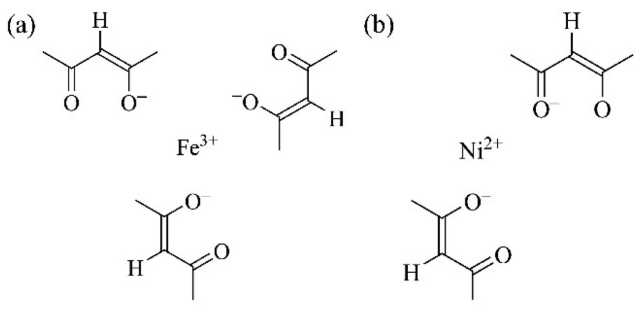

Fig. 1. Chemical structures of (a) $Fe(acac)_3$ and (b) $Ni(acac)_2$.

The internal structure of the high-pressure stainless steel vessel and the procedure for solubility measurements have been described in detail in our previous studies [35]. In a typical experiment, a certain amount of solute sealed in a filter-paper bag was placed in the porous cylindrical storage frame made of stainless steel, which was in turn installed in the upper part of the stainless steel vessel. The high-pressure vessel was then closed and placed in the thermostatic blast drying oven to preheat at the desired temperature for 2 h. Afterwards, the inlet and outlet needle valves were opened to replace the air in the reactor with CO_2. CO_2 was then introduced into the vessel to reach the target pressure with a pressurized system. The vessel was kept at constant pressure and temperature for a specified time (about 24 h), during which electromagnetic stirring was used to improve mixing efficiency and reach dissolution equilibrium. Finally, the outlet valve was opened to quickly release the CO_2 from the vessel. Then, the filter-paper bag containing the undissolved salt was removed and weighed. The amount of dissolved solute was easily obtained as the mass difference of the filter-paper bag, and solubility was determined as the ratio of dissolved solute to the $scCO_2$ volume under the given pressure and temperature conditions.

A longer equilibration time maybe required to ensure complete dissolution of the precursor in $scCO_2$. Therefore, the dissolution time was extended to 48 h. The measured solubility data as shown in Fig. 3 is in good agreement with the solubility isotherms, which proved that 24 h is sufficient to achieve dissolution equilibrium.

3. Results and Discussion

3.1. Solubility of $Fe(acac)_3$

Experimental results for the solubilities of $Fe(acac)_3$ in $scCO_2$ at temperatures ranging from 313.15 to 333.15 K are listed in Table 1, and solvent densities were obtained from NIST (National Institute of Standards and Technology). The experimental results for Fe $(acac)_3$ depicted in Fig. 4 were in general agreement with the solubility data reported in the literature. Considering the numerical magnitude of solubility, the present work was close to the measurements of Haruki *et al.* [32] and between those of Roggeman *et al.* [31] and Andersen *et al.* [33]. The average absolute relative deviations (AARD) between the solubility isotherm of this work at 313.15 K and literature data were 2.63%, 6.71%, and 15.66%, respectively, when pressure exceeded 10.6 MPa. The AARD were 16.12%, 14.41%, and 25.40% at 333.15 K and pressure of more than 13.8 MPa, respectively. In addition, the isotherm of the present work at 323.15 K was significantly higher than the solubility data of Andersen *et al.* [33] with AARD of 69.37%.

The effects of temperature and pressure on the solubility of Fe $(acac)_3$ in $scCO_2$ were analyzed. For a given temperature, the solubility increases with pressure due to the higher density of the solvent. A crossover region of solubility isotherms with pressure is observed at the pressure range studied. The range of this region calculated from a semi-empirical model associated with experimental data is 16.34–19.08 MPa. Below this range, the solubility decreases with temperature due to the decrease in solvent density. When the pressure exceeds 19.08 MPa, solubility increases with temperature due to the increase in the solute vapor pressure.

3.2. Solubility of $Ni(acac)_2$

Experimental results for the solubilities of $Ni(acac)_2$ in $scCO_2$ at temperatures ranging from 313.15 to 333.15 K are listed in Table 2. The experimental results of $Ni(acac)_2$ are also described in Fig. 5 along with the solubilities reported in the literature. The solubility isotherm of the present work at 333.15 K deviated significantly

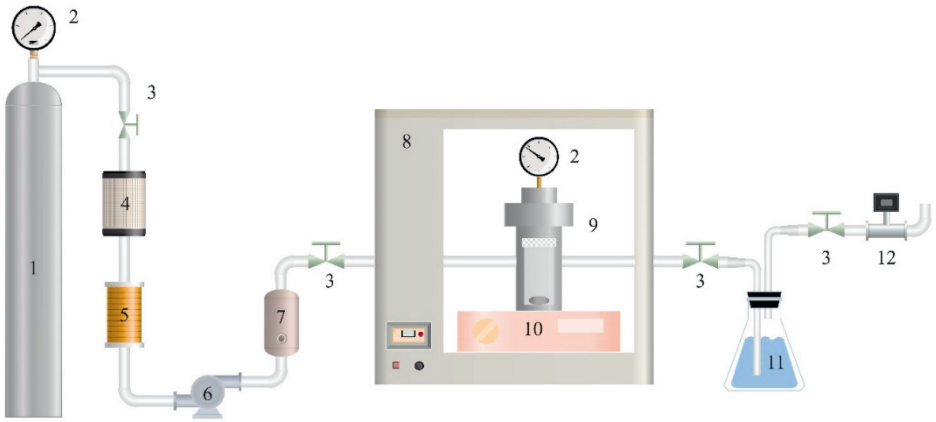

Fig. 2. Experimental equipment: (1) high purity carbon dioxide cylinder; (2) pressure sensor; (3) high precision needle valve; (4) CO_2 filter; (5) cooling coil; (6) high-pressure liquid chromatography (HPLC) pump; (7) buffer vessel; (8) thermostatic blast drying oven; (9) high-pressure stainless-steel vessel; (10) magnetic stirrer; (11) cold trap; (12) wet gas meter.

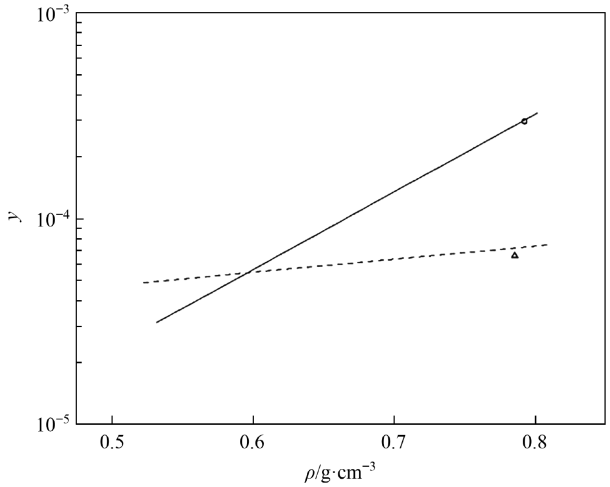

Fig. 3. Experimental solubilities of $Fe(acac)_3$ and $Ni(acac)_2$ in $scCO_2$ for a dissolution time of 48 h. ○, $Fe(acac)_3$, at 323.15 K and 20.7 MPa; △, $Ni(acac)_2$, at 323.15 K and 20.1 MPa; (—), solubility isotherm of $Fe(acac)_3$ at 323.15 K for a dissolution time of 24 h; (- - -), solubility isotherm of $Ni(acac)_2$ at 323.15 K for a dissolution time of 24 h.

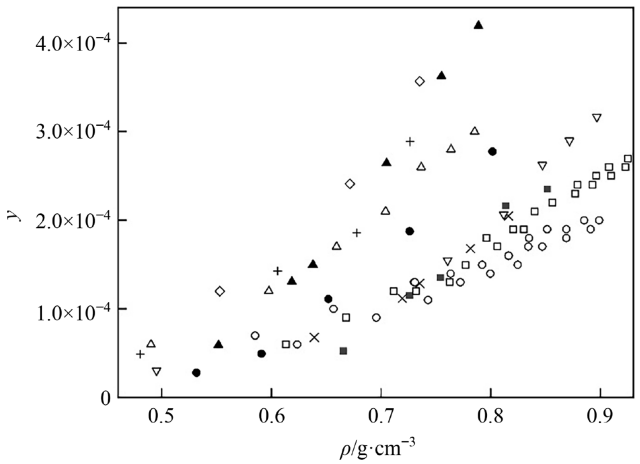

Fig. 4. Experimental solubilities of $Fe(acac)_3$ in $scCO_2$. ■, ●, ▲, this work at 313.15, 323.15, and 333.15 K; ×, +, Haruki *et al.* [32] at 313 and 333 K; ▽, ◇, Roggeman *et al.* [31] at 313.15 and 333.15 K; □, ○, △, Andersen *et al.* [33] at 313, 323, and 333 K.

Table 1
Experimental solubility data for $Fe(acac)_3$ in $scCO_2$

T/K	P/MPa	ρ/kg·m^{-3}	S/g·L^{-1}	y
313.15	10.6	665.33	0.28	0.52×10^{-4}
313.15	12.3	726.04	0.67	1.16×10^{-4}
313.15	13.5	753.64	0.82	1.35×10^{-4}
313.15	17.5	813.83	1.42	2.17×10^{-4}
313.15	21.3	851.39	1.61	2.35×10^{-4}
323.15	11.3	531.74	0.12	0.28×10^{-4}
323.15	12.1	590.89	0.23	0.49×10^{-4}
323.15	13.4	651.87	0.58	1.11×10^{-4}
323.15	16.2	726.09	1.09	1.88×10^{-4}
323.15	20.7	792.56	1.89	2.98×10^{-4}
323.15	21.5	801.38	1.79	2.78×10^{-4}
333.15	13.8	551.36	0.26	0.59×10^{-4}
333.15	15.4	618.38	0.65	1.31×10^{-4}
333.15	16.0	637.50	0.77	1.50×10^{-4}
333.15	18.9	704.86	1.50	2.64×10^{-4}
333.15	22.2	754.94	2.20	3.62×10^{-4}
333.15	25.2	788.56	2.66	4.20×10^{-4}

Table 2
Experimental solubility data for $Ni(acac)_2$ in $scCO_2$

T/K	P/MPa	ρ/kg·m^{-3}	S/g·L^{-1}	y
313.15	9.5	580.01	0.75×10^{-1}	2.20×10^{-5}
313.15	10.6	665.33	1.14×10^{-1}	2.94×10^{-5}
313.15	14.0	763.27	1.54×10^{-1}	3.44×10^{-5}
313.15	15.6	789.27	1.65×10^{-1}	3.58×10^{-5}
313.15	18.9	829.07	2.13×10^{-1}	4.39×10^{-5}
313.15	21.0	848.81	2.21×10^{-1}	4.46×10^{-5}
323.15	11.2	522.51	1.51×10^{-1}	4.94×10^{-5}
323.15	11.8	571.43	1.68×10^{-1}	5.02×10^{-5}
323.15	13.8	665.78	2.60×10^{-1}	6.69×10^{-5}
323.15	17.8	755.59	2.77×10^{-1}	6.29×10^{-5}
323.15	20.1	785.51	3.03×10^{-1}	6.60×10^{-5}
323.15	22.4	810.64	3.66×10^{-1}	7.74×10^{-5}
333.15	12.9	498.89	2.27×10^{-1}	7.81×10^{-5}
333.15	14.5	584.13	2.73×10^{-1}	8.01×10^{-5}
333.15	16.3	646.19	3.11×10^{-1}	8.25×10^{-5}
333.15	20.0	723.68	3.51×10^{-1}	8.30×10^{-5}
333.15	24.5	781.41	3.76×10^{-1}	8.24×10^{-5}

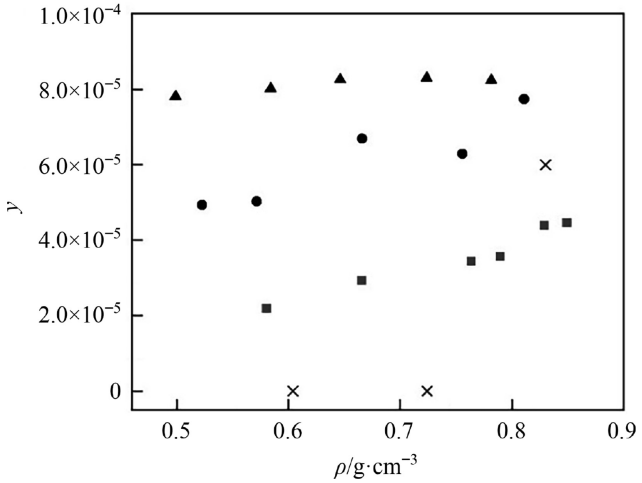

Fig. 5. Experimental solubilities of Ni(acac)$_2$ in scCO$_2$. ■, ●, ▲, this work at 313.15, 323.15, and 333.15 K; ×, Aschenbrenner *et al.* [28] at 333 K.

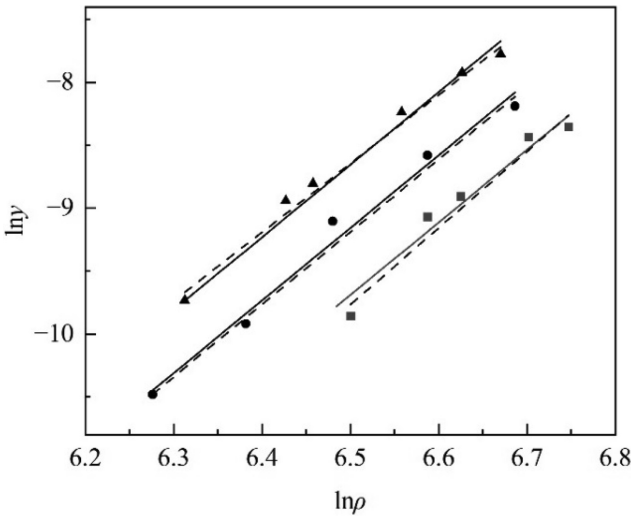

Fig. 6. Relationship between the logarithm of the molar fraction solubility of Fe(acac)$_3$ and the logarithm of the density of scCO$_2$. ■, ●, ▲, this work at 313.15, 323.15, and 333.15 K; (—), Eq. (1); (- - -), Eq. (2).

from the experimental solubility of Aschenbrenner *et al.* [28] with AARD of 47.4% at 30 MPa. Furthermore, the solubility measured at 313 K and 16 MPa by Kersch *et al.* [34] was approximately two orders of magnitude lower than the experimental results of the present work.

The effects of temperature and pressure on the solubility of Ni(acac)$_2$ were discussed. The solubility of Ni(acac)$_2$ presents a logarithmic relationship with pressure at the studied temperatures. The slope of the solubility isotherm decreases with increasing pressure. For a given pressure, the solubility increases with temperature.

3.3. Solubility data correlation

Solubility data for both systems were fitted to the semi-empirical equations proposed by Chrastil [36] and by Sung and Shim [37]. Chrastil model provides a linear relationship between the natural logarithms of the solubility, y and the solvent density, ρ (kg·m^{-3}), and is given by Eq. (1):

$$\ln y = a + \frac{b}{T} + k\ln\rho \tag{1}$$

where a, b and k are temperature independent adjustable parameters. In the original model a is related to the molecular mass of solute and solvent, b considers the heats of solvation and vaporization and k is an association number.

The semi-empirical model presented by Sung and Shim whose slope of the solubility isotherms decreases with increasing temperature provides a linear relationship between the natural logarithm of solubility and the solvent density given by Eq. (2):

$$\ln y = a + \frac{b}{T} + \left(c + \frac{d}{T}\right)\ln\rho \tag{2}$$

where a, b, c and d are all adjustable parameters independent of temperature.

The relationship between the molar fraction solubility of Fe(acac)$_3$ and the density of scCO$_2$ is illustrated on the double logarithmic chart in Fig. 6. Approximately linear relationships were obtained for the solubility isotherms, and the slopes of the isotherms were nearly identical. The correlation results for the solubilities of Fe(acac)$_3$ using Eqs. (1) and (2) are listed in Table 3. Reasonable correlation results were obtained using the empirical models proposed by Chrastil and Sung and Shim.

Table 3
Correlated results for the solubilities of Fe(acac)$_3$ using Eqs. (1) and (2)

Model	Parameter	T/K	AARD/%
Chrastil (Eq. (1))	a = −29.93	313.15	10.64
	b = −5406.21	323.15	9.10
	k = 5.77	333.15	6.69
		Total	8.68
Sung and Shim (Eq. (2))	a = 38.80	313.15	10.68
	b = −27611.10	323.15	8.18
	c = −4.60	333.15	6.87
	d = 3348.62	Total	8.47

The relationship between the molar fraction solubility of Ni(acac)$_2$ and the density of scCO$_2$ is illustrated on the double logarithmic chart in Fig. 7. Nearly linear behaviors were observed for the solubility isotherms, and the slope of the isotherms decreased with increasing temperature. The correlation results for the solubilities of Ni(acac)$_2$ using Eqs. (1) and (2) are listed in Table 4. The solubility data for Ni(acac)$_2$ correlated better with the semi-

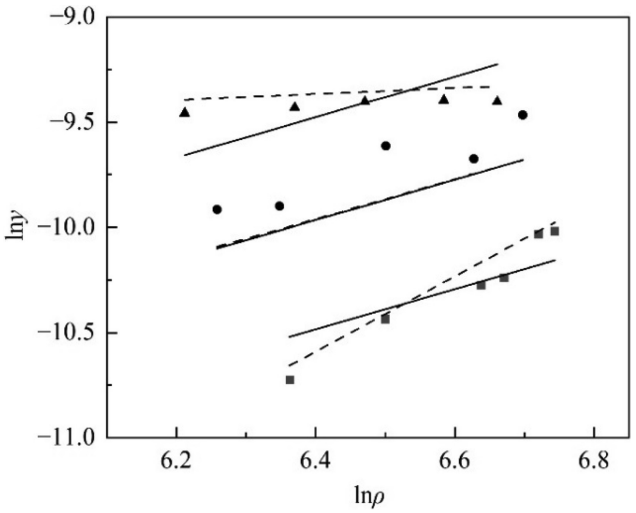

Fig. 7. Relationship between the logarithm of the molar fraction solubility of Ni(acac)$_2$ and the logarithm of the density of scCO$_2$. ■, ●, ▲, this work at 313.15, 323.15, and 333.15 K; (—), Eq. (1); (- - -), Eq. (2).

Table 4
Correlated results for the solubilities of $Ni(acac)_2$ using Eqs. (1) and (2)

Model	Parameter	T/K	AARD/%
Chrastil (Eq. (1))	a = 0.18	313.15	9.48
	b = −5263.87	323.15	15.32
	k = 0.96	333.15	11.06
		Total	11.80
Sung and Shim (Eq. (2))	a = 173.98	313.15	6.77
	b = −61387.53	323.15	15.02
	c = −25.65	333.15	6.28
	d = 8593.06	Total	9.20

empirical model proposed by Sung and Shim [37]. Reproducibility of the experimental isothermal solubility was 9.20% at its maximum and 15.02% as a whole.

3.4. Phase equilibrium experiment

In the solubility determination experiment, a large amount of brick-red $Fe(acac)_3$ could be clearly observed inside the high-pressure reactor after CO_2 removal, but green $Ni(acac)_2$ was only observed on the surface of the filter paper bag with a small amount, due to the difference in color and solubility of the two compounds. In order to visualized the dissolution process of metal complexes in $scCO_2$, the solubility experiment of $Fe(acac)_3$ was carried out at 313.15 K and 13 MPa using a phase equilibrium experimental apparatus. The experimental set-up has been described in our previous study [11]. In a typical experiment, the $Fe(acac)_3$ wrapped by filter paper was loaded into the reactor. A constant flow of high purity CO_2 was then slowly filled into the phase equilibrium cell with a plunger pump at 313.15 K until its pressure increased to 13 MPa.

The dissolution process of $Fe(acac)_3$ in $scCO_2$ is illustrated in Fig. 8. The initial state of the high-pressure reactor containing the sight glass without $scCO_2$ filling is shown in Fig. 8(a). After filling with $scCO_2$, the liquid level gradually raised (Fig. 8(b)) until it filled the whole viewport. Under the action of magnetic stirring, the unsaturated $scCO_2$ diffused into the filter paper bag, dissolving the $Fe(acac)_3$ inside and bringing it out. Due to the high solubility, the $scCO_2$ with dissolved $Fe(acac)_3$ showed a significant color change (from colorless to light yellow, Fig. 8(c)) after 15 min of dissolution. By extending the dissolution time, $scCO_2$ gradually changed from light yellow to dark yellow (Fig. 8(d)). Eventually, the $scCO_2$ with dissolved $Fe(acac)_3$ exhibited the original red color of $Fe(acac)_3$ (Fig. 8(e)). Rapidly removing $scCO_2$ from the system, a large amount of brick-red $Fe(acac)_3$ precipitated and dispersed in the bottom of the cavity (Fig. 8(f)).

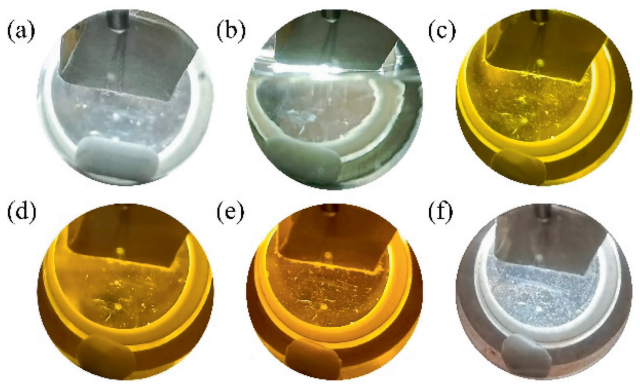

Fig. 8. Changes of $Fe(acac)_3$ in $scCO_2$ with dissolution time: (a) initial state without $scCO_2$ filling; (b) state during $scCO_2$ filling; (c) state after 15 min of $Fe(acac)_3$ dissolution in $scCO_2$; (d) state after 1 h of dissolution; (e) state after 4 h of dissolution; (f) state after pressure removal.

4. Conclusions

In this work, the solubilities of $Fe(acac)_3$ and $Ni(acac)_2$ in $scCO_2$ were measured using a static mass loss method. The molar fraction solubility values ranged from 0.28×10^{-4} to 4.20×10^{-4} and 2.20×10^{-5} to 8.30×10^{-5}, respectively, in wide ranges of pressure (9.5–25.2 MPa) and temperature (313.15–333.15 K). The solubility data obtained can be used to guide the materials preparation by supercritical fluid deposition method and is also the basic data for supercritical fluid chemical engineering. In double logarithmic plots, approximately linear relationships were observed for the solubility isotherms of both $Fe(acac)_3$ and $Ni(acac)_2$. The slope of the former was almost equal and independent of temperature, while the slope of the latter decreased with increasing temperature. The experimental solubility data were successfully correlated using the empirical models proposed by Chrastil and Sung and Shim. In the solubility determination experiments, a large amount of brick-red $Fe(acac)_3$ was clearly observed in the high-pressure reactor after the removal of CO_2. In order to visualize the dissolution process of the metal complexes in $scCO_2$, a high-pressure reactor with a viewable window was again used to perform the experiment.

Data Availability

Data will be made available on request.

Declaration of Competing Interest

The authors declare that they have no known competing financial interests or personal relationships that could have appeared to influence the work reported in this paper.

Acknowledgements

The authors are appreciative of financial support from the National Key Research and Development Program of China (2020YFA0710202), the National Natural Science Foundation of China (21978043, U1662130), Inner Mongolia University of Technology Scientific Research Initial Funding (DC2300001240), Talent Introduction Support Project of Inner Mongolia (DC2300001426).

References

[1] E.J. Beckman, Supercritical and near-critical CO_2 in green chemical synthesis and processing, *J. Supercrit. Fluids* 28 (2–3) (2004) 121–191.
[2] N.G. Smart, T. Carleson, T. Kast, A.A. Clifford, M.D. Burford, C.M. Wai, Solubility of chelating agents and metal-containing compounds in supercritical fluid carbon dioxide, *Talanta* 44 (2) (1997) 137–150.
[3] C.M. Wai, S. Wang, Separation of metal chelates and organometallic compounds by SFC and SFE/GC, *J. Biochem. Biophys. Meth.* 43 (1–3) (2000) 273–293.
[4] K.E. Laintz, C.M. Wai, C.R. Yonker, R.D. Smith, Extraction of metal ions from liquid and solid materials by supercritical carbon dioxide, *Anal. Chem.* 64 (22) (1992) 2875–2878.
[5] Y.H. Lin, C.M. Wai, Supercritical fluid extraction of lanthanides with fluorinated.beta.-diketones and tributyl phosphate, *Anal. Chem.* 66 (13) (1994) 1971–1975.
[6] J.Z. Yin, Q.Q. Xu, A.Q. Wang, Controlled growth of copper nanoparticles and nanorods in the channels of SBA-15 by supercritical fluid deposition, *Chem. Eng. Commun.* 197 (4) (2009) 627–632.
[7] I. Ushiki, N. Takahashi, T. Shimizu, Y. Sato, M. Ota, R.L. Smith, H. Inomata, Adsorption equilibria of rhodium acetylacetonate with MCM-41, MSU-H, and HMS silica substrates in supercritical carbon dioxide for preparing catalytic mesoporous materials, *J. Supercrit. Fluids* 120 (2017) 240–248.
[8] M.J. Tenorio, A. Cabañas, C. Pando, J.A.R. Renuncio, Solubility of $Pd(hfac)_2$ and $Ni(hfac)_2{\cdot}2H_2O$ in supercritical carbon dioxide pure and modified with ethanol, *J. Supercrit. Fluids* 70 (2012) 106–111.

[9] S. De Dea, D. Graziani, D.R. Miller, R.E. Continetti, Growth of magnetic thin films using CO_2 RESS expansions, *J. Supercrit. Fluids* 42 (3) (2007) 410–418.
[10] R.H. Guo, X.L. Jing, L.H. Peng, J.W. Lan, S.X. Jiang, W.Q. Yan, Nickel-catalyzed deposition of Cu film on PET fabric with supercritical fluid, *J. Mater. Sci.* 28 (22) (2017) 16618–16626.
[11] J.L. Qi, Q.Q. Xu, D. Zhou, J.Z. Yin, Q.K. Jiang, Preparation of Cu single atoms on N-doped carbon materials with supercritical CO_2 deposition, *J. Supercrit. Fluids* 171 (2021) 105202.
[12] J.L. Qi, D. Zhou, Q.Q. Xu, J.Z. Yin, K.P. Yu, H.X. Sun, Preparation of Pd-ZIF-8 single-atom catalyst with supercritical CO_2 deposition method, *Micropor. Mesopor. Mater.* 346 (2022) 112287.
[13] J.A. Darr, M. Poliakoff, New directions in inorganic and metal–organic coordination chemistry in supercritical fluids, *Chem. Rev.* 99 (2) (1999) 495–542.
[14] C.M. Wai, B. Waller, Dissolution of metal species in supercritical fluids principles and applications, *Ind. Eng. Chem. Res.* 39 (12) (2000) 4837–4841.
[15] J. Morère, M.J. Tenorio, C. Pando, J.A.R. Renuncio, A. Cabañas, Solubility of two metal–organic ruthenium precursors in supercritical CO_2 and their application in supercritical fluid technology, *J. Chem. Thermodyn.* 58 (2013) 55–61.
[16] I. Ushiki, R. Fujimitsu, S. Takishima, Predicting the solubilities of metal acetylacetonates in supercritical CO_2: Thermodynamic approach using PC-SAFT, *J. Supercrit. Fluids* 164 (2020) 104909.
[17] M. Ashraf-Khorassani, M.T. Combs, L.T. Taylor, Supercritical fluid extraction of metal ions and metal chelates from different environments, *J. Chromatogr. A* 774 (1–2) (1997) 37–49.
[18] J.H. Aubert, Solubility of carbon dioxide in polymers by the quartz crystal microbalance technique, *J. Supercrit. Fluids* 11 (3) (1998) 163–172.
[19] S. Yoda, Y. Mizuno, T. Furuya, Y. Takebayashi, K. Otake, T. Tsuji, T. Hiaki, Solubility measurements of noble metal acetylacetonates in supercritical carbon dioxide by high performance liquid chromatography (HPLC), *J. Supercrit. Fluids* 44 (2) (2008) 139–147.
[20] B. Li, W. Guo, H.J. Chi, Z.Q. Zhang, E.D. Ramsey, Key measurements performed using on-line supercritical fluid chromatography to support process design and development, *Trac. Trends Anal. Chem.* 146 (2022) 116479.
[21] M. Haruki, F. Kobayashi, K. Kishimoto, S.I. Kihara, S. Takishima, Measurement of the solubility of metal complexes in supercritical carbon dioxide using a UV–vis spectrometer, *Fluid Phase Equilib.* 280 (1–2) (2009) 49–55.
[22] M. Haruki, M. Ohara, S.I. Kihara, S. Takishima, Solubilities of cobalt(III) and chromium(III) acetylacetonates in supercritical carbon dioxide at elevated temperatures, *Fluid Phase Equilib.* 357 (2013) 50–56.
[23] S.E. Guigard, G.L. Hayward, R.G. Zytner, W.H. Stiver, Measurement of solubilities in supercritical fluids using a piezoelectric quartz crystal, *Fluid Phase Equilib.* 187–188 (2001) 233–246.
[24] M. Škerget, Ž. Knez, M. Knez-Hrnčič, Solubility of solids in sub- and supercritical fluids: A review, *J. Chem. Eng. Data* 56 (4) (2011) 694–719.
[25] H.B. Rad, J.K. Sabet, F. Varaminian, Study of solubility in supercritical fluids: Thermodynamic concepts and measurement methods—A review, *Braz. J. Chem. Eng.* 36 (4) (2019) 1367–1392.
[26] W.H. Teoh, R. Mammucari, N.R. Foster, Solubility of organometallic complexes in supercritical carbon dioxide: A review, *J. Organomet. Chem.* 724 (2013) 102–116.
[27] Ž. Knez, D. Cör, M. Knez Hrnčič, Solubility of solids in sub- and supercritical fluids: A review 2010–2017, *J. Chem. Eng. Data* 63 (4) (2018) 860–884.
[28] O. Aschenbrenner, S. Kemper, N. Dahmen, K. Schaber, E. Dinjus, Solubility of β-diketonates, cyclopentadienyls, and cyclooctadiene complexes with various metals in supercritical carbon dioxide, *J. Supercrit. Fluids* 41 (2) (2007) 179–186.
[29] M. Haruki, F. Kobayashi, S.I. Kihara, S. Takishima, Solubility of β-diketonate complexes of copper(II) and cobalt(II) in supercritical carbon dioxide, *J. Chem. Eng. Data* 56 (5) (2011) 2230–2235.
[30] A. Lagalante, B. Hansen, T. Bruno, R. Sievers, Solubilities of copper(II) and chromium(III) beta-diketonates in supercritical carbon-dioxide, *Inorg. Chem.* 34 (1995) 5781–5785.
[31] E.J. Roggeman, A.M. Scurto, J.F. Brennecke, Spectroscopy, solubility, and modeling of cosolvent effects on metal chelate complexes in supercritical carbon dioxide solutions, *Ind. Eng. Chem. Res.* 40 (3) (2001) 980–989.
[32] M. Haruki, F. Kobayashi, S.I. Kihara, S. Takishima, Effect of the chemical structures of iron complexes on the solubilities in supercritical carbon dioxide, *Fluid Phase Equilib.* 308 (1–2) (2011) 1–7.
[33] W.C. Andersen, R.E. Sievers, A.F. Lagalante, T.J. Bruno, Solubilities of cerium (IV), terbium(III), and iron(III) β-diketonates in supercritical carbon dioxide, *J. Chem. Eng. Data* 46 (5) (2001) 1045–1049.
[34] C. Kersch, G.J. Witkamp, G.F. Woerlee, Supercritical fluid extraction: A study on metal recovery and regeneration of β-diketones and organophosphorus extractants, *Solvent Extr. Ion Exch.* 23 (2) (2005) 189–212.
[35] J.L. Qi, Q.Q. Xu, J.F. Sun, D. Zhou, J.Z. Yin, An extraction-based facile method for measuring the solubility of organic solid compounds in supercritical carbon dioxide, *Chem. Eng. Commun.* 210 (1) (2023) 137–145.
[36] J. Chrastil, Solubility of solids and liquids in supercritical gases, *J. Phys. Chem.* 86 (15) (1982) 3016–3021.
[37] H.D. Sung, J.J. Shim, Solubility of C. I. disperse red 60 and C. I. disperse blue 60 in supercritical carbon dioxide, *J. Chem. Eng. Data* 44 (5) (1999) 985–989.